ARTICLE

Silver-Coated Silica Beads Applicable as Core Materials of Dual-Tagging Sensors Operating via SERS and MEF

Kwan Kim,*,† Yoon Mi Lee,† Hyang Bong Lee,† and Kuan Soo Shin*,‡

Department of Chemistry, Seoul National University, Seoul 151-742, Korea, and Department of Chemistry, Soongsil University, Seoul 156-743, Korea

ABSTRACT We have developed dual-tagging sensors, operating via both surface-enhanced Raman scattering (SERS) and metal-enhanced fluorescence (MEF), composed of silver-coated silica beads onto which were deposited SERS markers and dye-grafted polyelectrolytes, for multiplex immunoassays. Initially, a very simple electroless-plating method was applied to prepare Ag-coated silica beads. The Raman markers were then assembled onto the Ag-coated silica beads, after which they were brought to stabilization by the layer-by-layer deposition of anionic and cationic polyelectrolytes including a dye-grafted polyelectrolyte. In the final stage, the dual-tagging sensors were assembled onto them with specific antibodies (antihuman-IgG or antirabbit-IgG) to detect target antigens (human-IgG or rabbit-IgG). The MEF signal was used as an immediate indicator of molecular recognition, while the SERS signals were subsequently used as the signature of specific molecular interactions. For this reason, these materials should find wide application, especially in the areas of biological sensing and recognition that rely heavily on optical and spectroscopic properties.

KEYWORDS: surface-enhanced Raman scattering • metal-enhanced fluorescence • silica bead • layer-by-layer deposition • multiplex immunoassay • antigen−antibody binding

1. INTRODUCTION

Immunoassays based on antigen−antibody binding are a powerful analytical tool for biochemical studies, clinical diagnostics, and environmental monitoring (1−3). Many different immunoassay readout techniques such as scintillation counting, fluorescence, chemiluminescence, electrochemical and enzymatic methods, and Raman scattering have been successfully exploited for the detection of the antigen−antibody binding (4−10). Among these techniques, fluorescence is currently the principal detection method in bioassays, since high sensitivity is critical for immunoassay detection. It has, however, inherent drawbacks such as photobleaching, narrow excitation with broad emission profiles, and peak overlapping in multiplexed experiments. The latter limitations can be overcome by means of surface-enhanced Raman scattering (SERS) (11−16).

Raman scattering is a well-established vibrational spectroscopic method used in chemical analysis. However, generally its signals are too weak to be used for immunoassay, since most molecules exhibit low Raman scattering cross sections. SERS offers a chance to increase the Raman intensities of molecules adsorbed on nanostructured Au or Ag surfaces by about 6 orders or even 14 orders of magnitude, allowing the detection of the signal of a single molecule (17−20). In addition, SERS is insensitive to humidity, oxygen, and other quenchers and is thus a promising method for sensitive biological identifications and detections (21−23). Several groups have indeed developed various types of SERS-based materials that can be used in diagnostic bioassays (11, 13, 15, 24−27).

A significant increase in the fluorescence emission can also occur with nanostructured Ag and Au surfaces. The phenomenon, called surface-enhanced fluorescence (SEF) or metal-enhanced fluorescence (MEF), derives from the interaction of the dipole moment of the fluorophore and the surface plasmon field of the metal, resulting in an increase in the radiative decay rate and stronger fluorescence emission (28−36). In effect, this means that weakly emitting materials (dyes, proteins, or DNA) with low quantum yields can be transformed into more efficient fluorophores with a shortening of fluorescence lifetimes as well. The reduction in fluorescence lifetimes due to MEF means that molecules spend less time in the excited state, thus reducing photobleaching effects (31). These characteristics of the MEF effect therefore can be utilized in the development of efficient fluorescence-based sensors and microarrays (31, 37, 38).

Considering the sensitivity and specificity of assays, it would be desirable to develop dual-tag sensors operating as both SERS and fluorescence detection systems for multiple assays. The fluorescence signal might then be used as an immediate indicator of molecular recognition, while the SERS signals could be used subsequently as the signature of specific molecular interactions. In light of this consideration, we have recently examined the possibility of the simultaneous observation of SERS as well as fluorescence using rhodamine B isothiocyanate (RhBITC) as a probe molecule.

* To whom all correspondence should be addressed. K.K.: e-mail, kwankim@snu.ac.kr; tel, +82-2-8806651; fax, +82-2-8891568. K.S.S.: e-mail: kshin@ssu.ac.kr; tel, +82-2-8200436; fax, +82-2-8244383.
Received for review May 18, 2009 and accepted August 27, 2009
† Seoul National University.
‡ Soongsil University.
DOI: 10.1021/am9003396

Published on Web 09/15/2009

Scheme 1. Fabrication of a New Type of Dual-Tag Sensor, Operating via Both Raman (SERS) and Fluorescence (MEF) Spectroscopy, Composed of SiO_2@Ag Beads Modified with RhBITC Dye for Multiplex Immunoassays

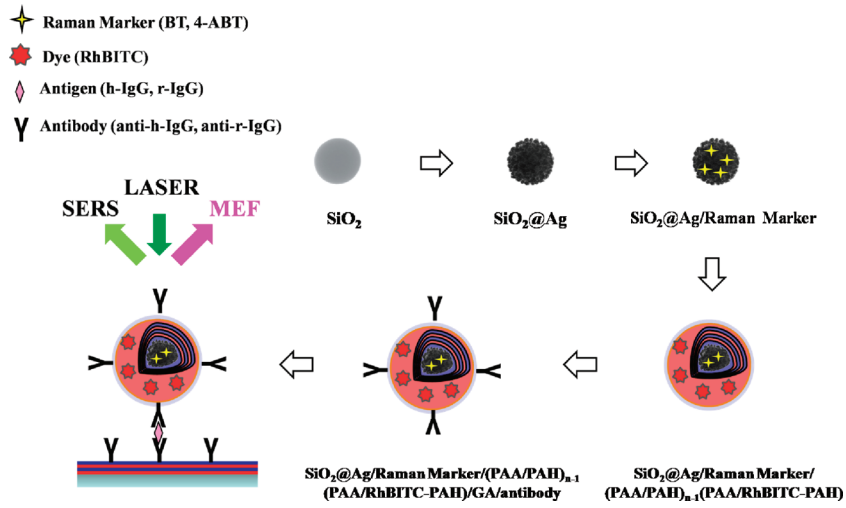

We in fact found that, once RhBITC is adsorbed onto Ag on silica or polystyrene beads, it exhibits not only a strong SERS signal of RhBITC but also a measurable amount of fluorescence (39). This indicates that both the fluorescence and SERS can be observed simultaneously for dye molecules adsorbed on metal nanoaggregates. Since such dye-modified silica or polystyrene beads were readily coated with polyelectrolytes for their further derivatization with biological molecules of interest that could bind to target molecules, they were expected to be useful, especially in the areas of biological sensing and recognition that should rely heavily on optical and spectroscopic means. In order to develop more versatile dual-tagging sensors, however, it would be better to use several Raman markers to distinguish the specific molecular interactions, even though the same dye molecule can be used as an immediate indicator of molecular recognition.

In this work, we have developed a dual-tag sensor operating via both SERS and MEF by derivatization of Raman-marker-adsorbed, Ag-coated silica beads with a dye-grafted polyelectrolyte. The strategy to assemble a dual-tag sensor for multiplex immunoassays is shown in Scheme 1. To our knowledge, this is the first report to observe simultaneously the SERS of ordinary Raman markers and MEF of dye molecules deposited on silica beads. The application prospects of these materials are expected to be very high, since the MEF signal can be used as an immediate indicator of molecular recognition, while the SERS signals are able to be used subsequently as the signature of specific molecular interactions.

2. EXPERIMENTAL SECTION

Chemicals. RhBITC (97%), silver nitrate (99%), butylamine (99%), poly(allylamine hydrochloride) (PAH, $M_w \approx 70$ kDa), poly(acrylic acid) (PAA, $M_w \approx 100$ kDa), tetraethyl orthosilicate (TEOS, 99%), benzenethiol (BT, 99+%), 4-aminobenzenethiol (4ABT, 97%), human-IgG (h-IgG), rabbit-IgG (r-IgG), goat antihuman-IgG (anti-h-IgG), mouse antirabbit-IgG (anti-r-IgG), glutaraldehyde (GA), and bovine serum albumin (BSA) were purchased from Aldrich and used as received. Other chemicals, unless specified, were of reagent grade. Highly pure water (Millipore Milli-Q system), of resistivity greater than 18.0 MΩ cm, was used throughout.

Preparation of Ag-Coated Silica (SiO_2@Ag) Beads. Monodispersed silica particles were prepared using the Stöber–Fink–Bohn method, comprising the base-catalyzed hydrolysis of TEOS in water–ethanol mixtures (40). When the silver was deposited onto the silica particles, the cleaned silica in ethanol was added into the silvering medium to a final concentration of 0.10 mg mL^{-1} (w/v, dried bead mass/ethanol) and then incubated for 50 min at 50 ± 1 °C with vigorous shaking. As a silvering mixture, the concentrations of $AgNO_3$ and butylamine were maintained at each 1 mM (39). After being rinsed with ethanol, the SiO_2@Ag beads were redispersed in ethanol under sonication for 5 min.

Labeling of PAH. PAH was covalently labeled with RhBITC (RhBITC-PAH). The reaction was performed in PAH solution (12.5 mg mL^{-1}) at pH 9.5 (buffered by sodium carbonate) by the addition of 0.4 wt % RhBITC with respect to the concentration of PAH. The product solution was separated by chromatography (Sephadex G25-150) (41, 42). From the molar extinction coefficient of RhBITC ($\varepsilon_o = 10.7 \times 10^4$ L mol^{-1} cm^{-1}) (41), the mean molar ratio of labeled monomers of PAH was estimated to be in the ratio 1:6150.

Derivatization of SiO_2@Ag with Raman Markers (SiO_2@Ag/Raman). In order to use SiO_2@Ag beads as a core material for molecular sensors operating via both SERS and MEF, first, 4ABT (or BT) molecules as a Raman marker were assembled onto the SiO_2@Ag beads and then the layer-by-layer (LbL) technique was applied to deposit spacer bilayers and a dye-modified bilayer onto them. Specifically, 0.1 mg of SiO_2@Ag beads was placed in a vial into which 10 mL of 1 mM ethanolic 4ABT (or BT) solution was subsequently added. After 3 h, the resulting solutions were centrifuged and then rinsed with ethanol to remove the excess Raman markers.

Further Derivatization of SiO_2@Ag/Raman with Polyelectrolytes. Four and a half bilayers of PAA and PAH were deposited initially onto SiO_2@Ag/Raman beads, and then the outermost PAA was reacted with RhBITC-PAH (in 2 mg mL^{-1}), via the LbL technique. Herein, a bilayer refers to the deposition of a pair of negative (PAA) and positive (PAH) polyelectrolyte layers. Polyelectrolyte layers were formed by the sequential dipping of the SiO_2@Ag/Raman beads into the PAA and PAH solutions (2 mg mL^{-1}) for 10 min at room temperature; the pH

of the PAH solution was 5.0, while that of the PAA solution was 4.2. In the interim, to change the polyelectrolyte solution, silica beads were intensively rinsed with water. In the final stage, the outermost layer, PAH, was derivatized further with molecular recognition units as described below.

Immobilization of Antibodies on Silica Beads To Detect Antigens. After one further bilayer of PAA and PAH was deposited, silica beads were shaken for 1 h in a 2.5% aqueous solution of GA, followed by washing with water and centrifugation (43−45). The resulting particles were incubated for 1 h in a PBS buffer containing 100 μg mL^{-1} anti-h-IgG (or anti-r-IgG) with shaking. After they were rinsed with PBS, these antibody-modified Ag-coated silica beads were redispersed in 2 mM Tris-HCl buffer solution containing 1% BSA (pH 7.2) and stored at 4 °C while not in use. For an immunoassay, two bilayers of PAA and PAH were separately assembled on a cleaned glass slide. Thereafter, the slide was successively incubated in a GA solution (2.5%) for 3 h, in a solution of anti-h-IgG (or anti-r-IgG) (100 μg mL^{-1}) for 12 h at 4 °C and then in a BSA (100 μg mL^{-1}) solution for 3 h. The antibody-modified slide was subsequently incubated for 30 min in a PBS buffer (pH 7.2) containing 1% BSA and different amounts of h-IgG antigen (or r-IgG antigen). The antigen-adsorbed substrate was thereafter immersed in a solution containing anti-h-IgG (or anti-r-IgG) modified Ag-coated silica beads for 3 h under gentle shaking. After washing with pure water, the modified glass slide was subjected to Raman spectroscopy and confocal laser scanning microscopy measurements.

Instrumentation. UV/vis absorption spectra were obtained using a SCINCO S-2130 spectrometer. Photoluminescence (PL) measurements were carried out on a JASCO FP-750 with an excitation wavelength of 514.5 nm. Confocal laser scanning microscopy (CLSM) images were captured with a Carl Zeiss-LSM510 equipped with a 543 nm line of a He/Ne laser and a water immersion objective. Field emission scanning electron microscopy (FE-SEM) images were obtained with a JSM-6700F field emission scanning electron microscope operated at 5.0 kV. Transmission electron microscopy (TEM) images were obtained on a JEM-200CX transmission electron microscope at 200 kV. To approximate the thickness of PAA/PAH bilayers on SiO_2@Ag beads, similar bilayers were separately assembled on an Ag-coated glass substrate, and their thickness was estimated using a Rudolph Auto EL II optical ellipsometer. As usual, the refractive index of the polyelectrolyte films was assumed to be 1.45 (46). At least five different sampling points were considered to get the averaged thickness value. The Raman spectral measurements were conducted using a Renishaw Raman system Model 2000 spectrometer equipped with an integral microscope (Olympus BH2-UMA). The 514.5 nm radiation from a 20 mW air-cooled Ar^+ laser (Melles-Griot Model 351MA520) and the 632.8 nm radiation from a 17 mW air-cooled He/Ne laser (Spectra Physics Model 127) were used as the excitation sources. Raman scattering was detected with 180° geometry using a Peltier cooled (−70 °C) charge-coupled device (CCD) camera (400 × 600 pixels). The data acquisition time was usually 30 s. The Raman band of a silicon wafer at 520 cm^{-1} was used to calibrate the spectrometer.

3. RESULTS AND DISCUSSION

Characterization of SiO_2@Ag Beads. According to the FE-SEM images, the silica (SiO_2) beads prepared in this work were spherical with a mean diameter of 250 ± 9 nm. Probably due to the termination with OH groups, the silica beads were readily dispersed in water and ethanol without aggregation. As described in the Experimental Section, Ag was deposited onto these silica beads by soaking in ethanolic solutions of $AgNO_3$ and butylamine (39, 47). Parts a and b of Figure 1 show the FE-SEM images taken before and after

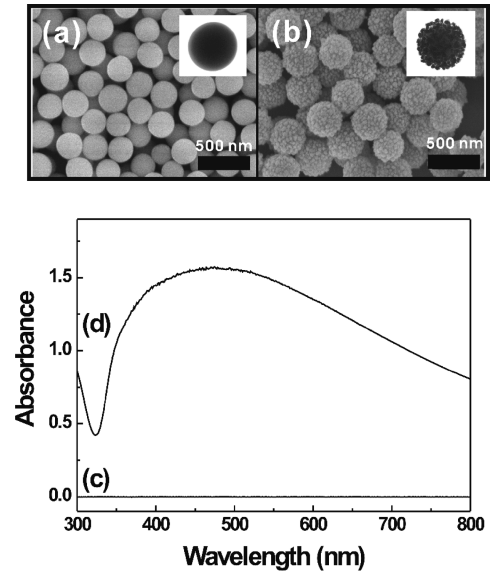

FIGURE 1. FE-SEM images taken (a) before and (b) after deposition of silver onto a 250 nm silica bead (scale bars represent 500 nm) and UV/vis extinction spectra of (c) bare SiO_2 and (d) SiO_2@Ag beads. SiO_2@Ag beads were prepared in a 1:1 mixture of $AgNO_3$ and butylamine. The inset of each panel shows the corresponding TEM image of a single silica bead.

deposition of silver onto silica beads, respectively. The deposition of networklike Ag could also be confirmed from the UV/vis spectra. Parts c and d of Figure 1 show the UV/vis extinction spectra of bare and Ag-coated silica beads, respectively. The spectrum measured for bare silica powder was featureless (Figure 1c). However, upon the deposition of silver, a very broad band appeared, extending from the near-UV to near-infrared regions due to a networklike Ag nanoaggregate formed on those powders (Figure 1d). Since the Ag surface formed in a 1:1 molar ratio of $AgNO_3$ and butylamine was the most SERS active (vide infra), the subsequent experiments were all carried out using those SiO_2@Ag beads.

Characterization of Dye-Modified SiO_2@Ag/Raman Beads. The next task was to find the optimum condition of the MEF. In fact, an extensive literature exists describing the MEF, and the fluorescence increase is known to occur at precise distances (5−30 nm) above nanoroughened metal surfaces (28, 31). We thus measured the fluorescence of RhBITC-labeled PAH as a function of its distance from the surface of Ag on SiO_2 beads. The latter distance was controlled by the number of PAA/PAH bilayers deposited onto the SiO_2@Ag beads beforehand. The polyelectrolytes can be deposited on any substrates irrespective of their surface charges. We discovered recently that polyelectrolytes such as anionic PAA and cationic PAH can be deposited consecutively not only onto hydrophilic surfaces but also onto hydrophobic surfaces (48). In order to estimate the actual thicknesses of polyelectrolyte layers, we assembled a series of PAA/PAH bilayers onto an Ag-coated glass substrate and then carried out ellipsometric thickness measurements. As can be seen in Figure 2, the ellipsometric thickness increased monotonically in proportion to the number of deposition cycles of PAA/PAH bilayers. Hence, in the case

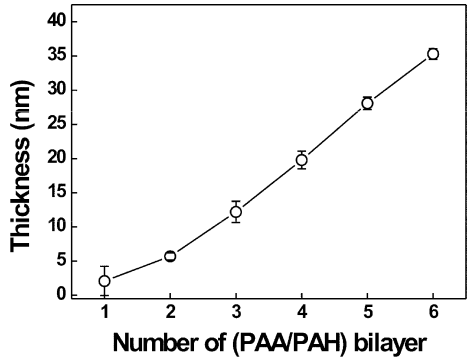

FIGURE 2. Ellipsometric thickness measured as a function of the (PAA/PAH) bilayers deposited onto a silver-coated glass substrate. The error bar indicates the standard deviation in triplicate experiments.

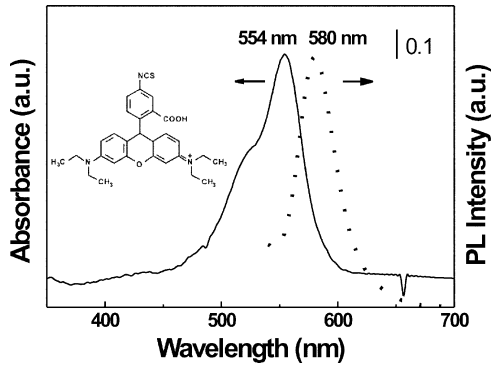

FIGURE 3. UV/vis absorption and PL spectra of 0.1 mM RhBITC-grafted PAH in a pH 9.5 aqueous solution. The inset shows the molecular structure of RhBITC.

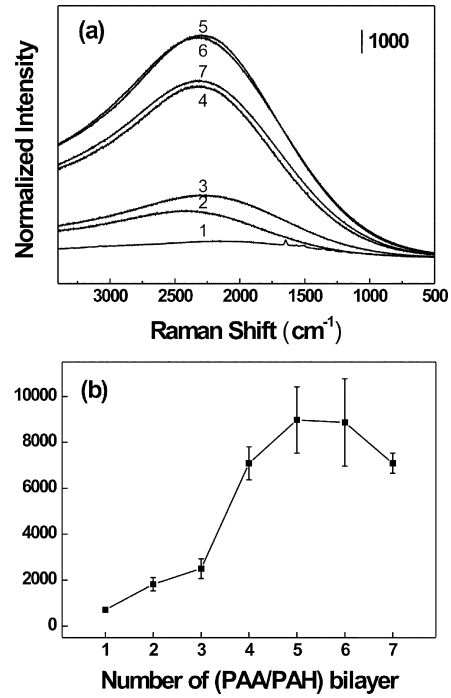

FIGURE 4. (a) Raman spectra taken as a function of the number of $(PAA/PAH)_{n-1}$(PAA/RhBITC-PAH) bilayers assembled on SiO_2@Ag beads. All spectra were taken using 514.5 nm radiation as the excitation source, and the background intensity was normalized with respect to that of a silicon wafer at 520 cm^{-1}. (b) Maximum Raman intensity at 2200 cm^{-1} plotted as a function of the number of $(PAA/PAH)_{n-1}$(PAA/RhBITC-PAH) bilayers assembled on SiO_2@Ag beads. All of the symbols shown are the average of 15 different measurements, with error bars denoting their standard deviation.

when five bilayers of PAA and PAH were deposited onto the Ag-coated silica beads, the actual thickness of polyelectrolytes could be approximated to be around 30 nm. On these grounds, we subsequently examined the MEF of RhBITC by Raman spectroscopy.

The molecular structure of RhBITC is shown in the inset of Figure 3. The solid and dotted lines in Figure 3 represent respectively the UV/vis absorption and PL spectra of 0.1 mM RhBITC-grafted PAH in a pH 9.5 aqueous solution; the absorption maximum is located at ~554 nm, while the emission maximum is located at ~580 nm. We now show in Figure 4a the Raman background spectra taken as a function of the number of $(PAA/PAH)_{n-1}$(PAA/RhBITC-PAH) layers assembled on Ag-coated silica beads; all spectra were taken using 514.5 nm radiation as the excitation source, and the background intensity was normalized with respect to that of a silicon wafer at 520 cm^{-1}. The maximum background peaks of the Raman spectra were observed around 2200 cm^{-1}, corresponding to the typical fluorescence peak of RhBITC dye at 580 nm. As shown in Figure 4a, when RhBITC molecules are directly in contact with Ag-coated silica beads ($n = 1$), distinct Raman peaks of RhBITC are observed due to the quenching of fluorescence. This clearly indicates that SiO_2@Ag beads are very efficient SERS-active substrates. However, those SERS peaks become invisibly weak when a spacer layer is present between the RhBITC and the Ag-coated beads. This indicates that the SERS intensity decreases dramatically with any increase in the distance between the adsorbate and the surface of metal. Nonetheless, the background intensities clearly increase as the thickness of the spacer layer increases. This must be due to MEF, becoming maximum when RhBITC is distant by five bilayers of PAA and PAH from Ag. From the measured ellipsometric thicknesses, the maximum MEF thus occurs at a distance of 30 nm from the surface of Ag-coated beads. The distance identified herein matches the literature values well (42). For clarity, the maximum Raman background intensities at 2200 cm^{-1} of $(PAA/PAH)_{n-1}$(PAA/RhBITC-PAH) layers assembled on Ag-coated silica beads are compared in Figure 4b, as a function of the number of (PAA/PAH) bilayers. The maximum Raman intensity of RhBITC on the Ag-coated silica beads with five spacer bilayers is nearly 8 times stronger than that of RhBITC-PAH adsorbed on Ag-coated silica beads without a spacer bilayer. Even though MEF enhancement is less than 10-fold in this study, it can be used as an immediate indicator of molecular recognition with a small amount of fluorescent dyes, while the SERS signals are able to be used subsequently as the signature of specific molecular interactions.

It should be pointed out that although SERS and MEF phenomena share a common electromagnetic enhancement mechanism, the SERS and MEF effects have opposite distance dependency on the nanostructured surface (28). SERS requires the molecule to have close contact with the metal surface, whereas MEF needs a certain distance from the surface of the metal nanostructure to prevent signal quench-

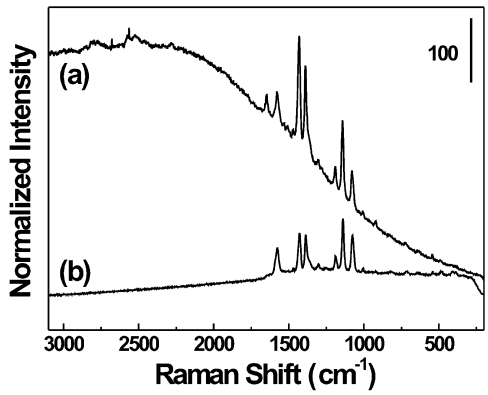

FIGURE 5. Raman spectra of RhBITC-modified SiO_2@Ag/4ABT beads taken using (a) 514.5 nm and (b) 632.8 nm radiation as the excitation source. The peak intensity was normalized with respect to that of a silicon wafer at 520 cm^{-1}.

ing. Fluorescence is quenched when the fluorophore is directly in contact with a metal surface due to nonradiative energy transfer from the excited state of the molecule to the metal. The excitation of plasmon resonances in the metal also produces enhancement of the local field in close proximity to the surface, which can lead to enhancement of different optical phenomena, including fluorescence (28, 31), as observed in this work.

In Figure 4b is seen that the maximum MEF at a distance of five bilayers of PAA and PAH is not excessively larger than the MEF at a distance of four bilayers. Accordingly, in subsequent work to realize a dual-tagging sensor, the RhBITC-labeled PAH was assembled onto the SiO_2@Ag beads only after the deposition of four and a half bilayers of PAA and PAH onto them. That is, initially two different SERS markers, i.e. BT and 4ABT, were adsorbed fully onto the SiO_2@Ag beads and then four and a half bilayers of PAA and PAH were deposited thereon. Subsequently, the outermost PAA was grafted with the RhBITC-PAH. To confirm the successful adsorption of SERS markers and dye-grafted polyelectrolytes, we took a series of Raman spectra using two different excitation sources. Parts a and b of Figure 5 show the Raman spectra taken using 514.5 and 632.8 nm radiation, respectively, for the system represented as (SiO_2@Ag/4ABT)(PAA/PAH)$_4$(PAA/RhBITC-PAH). In Figure 5a, a strong fluorescence background is identified around 2200 cm^{-1}. This must be due to the presence of RhBITC-PAH. When the Raman spectra are taken using 632.8 nm radiation as the excitation source, the fluorescence background is nearly invisible, however, as can be seen in Figure 5b. This is not unreasonable, since the excitation wavelength is obviously off the absorption profile of RhBITC shown in Figure 3. The SERS spectral pattern in Figure 5b is then exclusively due to 4ABT adsorbed on Ag. This must be so, since aliphatic polyelectrolytes are intrinsically weak Raman scatterers and also the SERS signals are expected to derive mostly from the first layer of the adsorbates such that PAA and PAH coated over 4ABT negligibly contribute to the measured Raman spectrum. The present observations clearly suggest that above SiO_2@Ag beads modified further with molecular recognition units can be used as a molecular sensor operating via both SERS and fluorescence. To confirm its feasibility, we have conducted additional experiments to differentiate the interaction of h-IgG with anti-h-IgG from that of r-IgG with anti-r-IgG.

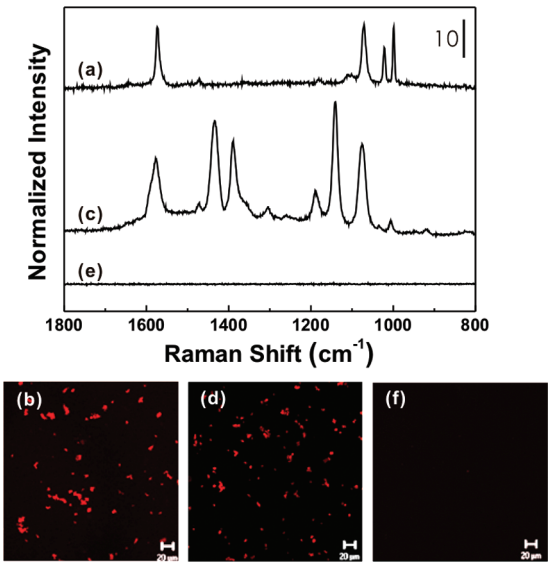

FIGURE 6. Raman spectra and CLSM images obtained after (a and b, respectively) anti-h-IgG modified SiO_2@Ag/BT beads had been allowed to interact via h-IgG with other anti-h-IgG modified layers on glass, (c and d, respectively) anti-r-IgG modified SiO_2@Ag/4ABT beads had been allowed to interact via r-IgG with other anti-r-IgG modified layers on glass, and (e and f, respectively) anti-r-IgG modified SiO_2@Ag/4ABT beads had been allowed to interact via h-IgG with other anti-r-IgG modified layers on glass. The Raman spectra were taken using 632.8 nm radiation as the excitation source. The scale bars in CLSM images represent 20 μm.

Detection of Antigen. As described in the Experimental Section, we first deposited one more bilayer of PAA and PAH onto (SiO_2@Ag/BT)(PAA/PAH)$_4$(PAA/RhBITC-PAH) and (SiO_2@Ag/4ABT)(PAA/PAH)$_4$(PAA/RhBITC-PAH), and then the outermost PAH was reacted with GA for the immobilization of anti-h-IgG and anti-r-IgG, respectively. These antibody-modified silica beads can be represented as either (SiO_2@Ag/BT)(PAA/PAH)$_4$(PAA/RhBITC-PAH)(PAA/PAH)(GA)(anti-h-IgG) or (SiO_2@Ag/4ABT)(PAA/PAH)$_4$(PAA/RhBITC-PAH)(PAA/PAH)(GA)(anti-r-IgG). Separately, we prepared nonfluorescent glass slides grafted in a similar way with anti-h-IgG or anti-r-IgG. (After the immobilization of antigens on both the silica beads and glass slides, they were treated with BSA to prevent nonspecific adsorption and to block any unreacted aldehyde groups.) The latter glass slides were subsequently immersed in a 10^{-4} g mL^{-1} solution of h-IgG or r-IgG for 30 min. Thereafter, these modified glass slides were incubated for 3 h in a solution containing the RhBITC-modified SiO_2@Ag/BT or SiO_2@Ag/4ABT beads, derivatized respectively with anti-h-IgG or anti-r-IgG. Parts a and b of Figure 6 show respectively the Raman spectrum and CLSM image obtained from the glass slide grafted initially with anti-h-IgG. The Raman peaks can be attributed to BT, illustrating that anti-h-IgG-grafted silica beads have interacted, via the mediation of h-IgG, with other anti-h-IgG assembled on a glass slide. Similarly, parts c and d of Figure 6 show, respectively, the Raman spectrum and CLSM image obtained from the glass slide grafted initially with anti-r-IgG. The Raman peaks can be attributed exclusively to 4ABT, indicating that anti-r-IgG-

grafted silica beads have bound, via the mediation of r-IgG, onto a glass slide grafted initially with anti-r-IgG. Parte e and f of Figure 6 represent respectively the Raman spectrum and CLSM image taken after a glass slide grafted initially with anti-r-IgG has been soaked consecutively in a solution containing h-IgG and then in a solution containing anti-r-IgG-grafted silica beads. In this case, no Raman peak or CLSM image was identified, suggesting that nonspecific binding was successfully avoided. These observations clearly support our claim that Ag-coated silica beads first adsorbing Raman markers thereon and then modifying further with fluorescent dye molecules can be used as core materials of dual-tagging sensors operating via both SERS and MEF. In specific terms, the enhanced fluorescence signal can be used as an immediate indicator of molecular recognition, while the SERS signals are used subsequently as the signature of specific molecular interactions.

In order to construct a dose–response curve for antigen, anti-r-IgG and r-IgG were chosen as a model system. Briefly, the substrate modified with anti-r-IgG was immersed in a solution containing different amounts of r-IgG, ranging from 10^{-4} to 10^{-11} g mL^{-1}. After incubation for 30 min at room temperature, the antigen-adsorbed substrate was immersed in a solution containing anti-r-IgG-modified SiO_2@Ag/Raman beads for 3 h with gentle shaking. By these processes, the antigen was first bound to the corresponding antibody immobilized beforehand on the substrate, and then it could capture the same antibody that has been immobilized on the SiO_2@Ag/Raman beads, as illustrated in Scheme 1. The SERS spectra obtained using 632.8 nm radiation at 30 s integration time (with the laser power at the sampling position being ~2 mW) is shown in Figure 7; the spectral feature is the same as that in Figure 6c. The SERS signals are from 4-ABT, and their intensities varied with different concentrations of r-IgG. The Raman spectral intensities decreased with the decrease of r-IgG concentrations, and fairly intense Raman spectra are obtained as long as the r-IgG concentrations are above 10^{-10} g mL^{-1}.

There have been many interesting reports about the encoded particles as a method of labeling antibodies and similar systems with different approaches (49–57). Recently, Huang et al. (49) developed novel Raman tags called nanoaggregate-embedded beads, which produce intense SERS signatures from the embedded Raman reporters. They demonstrated that these SERS-active beads could be used as Raman tags for biodetection. Sanles-Sobrido et al. (50) reported a synthetic approach for the development of multifunctional submicrometer reactors comprising catalytic Au nanoparticles confined inside hollow silica capsules. They also demonstrated that their complex nanostructures could be developed into SERS-encoded submicrometer particles for use in antigen biosensing. In the present investigation, we have developed a new type of dual-tag sensor operating via both SERS and MEF for immunoassays. Our method is unique in that the MEF signal can be used as an immediate indicator of molecular recognition, while the SERS signals are able to be used subsequently as the signature of specific molecular interactions. Many different kinds of dual-tagging sensors can also be developed by combinations of various Raman markers with several fluorescence dyes for immunoassays.

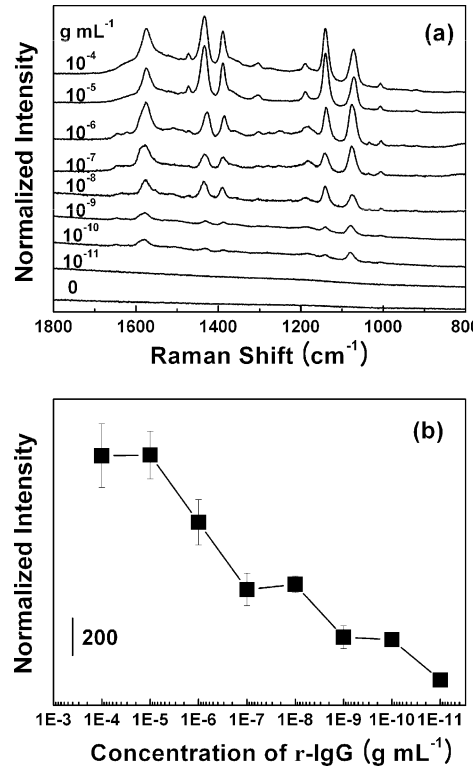

FIGURE 7. (a) SERS spectra of 4ABT measured after anti-r-IgG modified SiO_2@Ag/4ABT beads had been exposed to interact via different amounts of r-IgG with another anti-r-IgG-modified glass slide. (b) Normalized SERS intensity of the characteristic band of 4ABT at 1143 cm^{-1} measured as a function of concentrations of r-IgG. The SERS intensities were the average of five different measurements.

4. CONCLUSIONS

We have developed a new type of dual-tag sensor, operating via both SERS and MEF, for immunoassays. Initially, a very simple electroless-plating method was applied to prepare Ag-coated silica beads. After Raman labels were adsorbed (BT or 4ABT), PAA and PAH were deposited onto them by the LBL method: the beads became fluorescent due to the incorporation of RhBITC-grafted PAH in the latter process. In the final stage, the outermost PAH was reacted with GA, and then either anti-h-IgG or anti-r-IgG was immobilized thereon. Thereafter, we confirmed, by monitoring the SERS peaks of BT and the CLMS of RhBITC, that anti-h-IgG-grafted SiO_2@Ag particles interact exclusively with h-IgG. Similarly, we confirmed from the SERS peaks of 4ABT, as well as the CLMS of RhBITC, that anti-r-IgG-grafted SiO_2@Ag beads interact solely with r-IgG. These clearly illustrate that first, the binding event of the target molecule and then the specific type of antigen can be recognized consecutively by MEF and SERS, respectively. We also confirmed that antibody-grafted SiO_2@Ag particles could recognize antigens down to 10^{-10} g mL^{-1} solely by the SERS peaks of embedded Raman labels. The application prospects of these materials are thus expected to be very high,

especially in the areas of biological sensing and recognition that rely heavily on optical and spectroscopic properties.

Acknowledgment. This work was supported by the Korea Science and Engineering Foundation (Grant No. R11-2007-012-02002-0) and the Korea Research Foundation (Grant KRF-2008-313-C00390 and KRF-2008-313-C00411).

REFERENCES AND NOTES

(1) Ma, Z.; Sui, S. F. *Angew. Chem., Int. Ed.* **2002**, *41*, 2176–2179.
(2) Shuping, S.; Xiaohuo, J.; Weiqing, X.; Bing, Z.; Xiaoming, D.; Yubai, B.; Yukihiro, O. *J. Biomed. Opt.* **2005**, *10*, 0311121-1-12.
(3) Płaza, G.; Ulfig, K.; Tien, A. J. *Pol. J. Environ. Stud.* **2000**, *9*, 231–236.
(4) Gutcho, S.; Mansbach, L. *Clin. Chem.* **1977**, *23*, 1609–1614.
(5) Vuori, J.; Rasi, S.; Takala, T.; Vaananen, K. *Clin. Chem.* **1991**, *37*, 2087–2092.
(6) Brown, C. R.; Higgins, K. W.; Frazer, K.; Schoelz, L. K.; Dyminski, J. W.; Marinkovich, V. A.; Miller, S. P.; Burd, J. F. *Clin. Chem.* **1985**, *31*, 1500–1505.
(7) Hayes, F. J.; Halsall, H. B.; Heineman, W. R. *Anal. Chem.* **1994**, *66*, 1860–1865.
(8) Butler, J. E. *J. Immunoassay Immunoch.* **2000**, *21*, 165–209.
(9) Dou, X.; Takama, T.; Yamaguchi, Y.; Yamamoto, H.; Ozaki, Y. *Anal. Chem.* **1997**, *69*, 1492–1495.
(10) Ni, J.; Lipert, R. J.; Dawson, G. B.; Porter, M. D. *Anal. Chem.* **1999**, *71*, 4903–4908.
(11) Cao, Y. C.; Jin, R.; Mirkin, C. A. *Science* **2002**, *297*, 1536–1540.
(12) Cui, Y.; Ren, B.; Yao, J. L.; Gu, R. A.; Tian, Z. Q. *J. Phys. Chem. B* **2006**, *110*, 4002–4006.
(13) Grubisha, D. S.; Lipert, R. J.; Park, H. Y.; Driskell, J.; Porter, M. D. *Anal. Chem.* **2003**, *75*, 5936–5943.
(14) Kneipp, J.; Kneipp, H.; Rice, W. L.; Kneipp, K. *Anal. Chem.* **2005**, *77*, 2381–2385.
(15) Mulvaney, S. P.; Musick, M. D.; Keating, C. D.; Natan, M. J. *Langmuir* **2003**, *19*, 4784–4790.
(16) Su, X.; Zhang, J.; Sun, L.; Koo, T. W.; Chan, S.; Sundararajan, N.; Yamakawa, M.; Berlin, A. A. *Nano Lett.* **2005**, *5*, 49–54.
(17) Kneipp, K.; Wang, Y.; Kneipp, H.; Perelman, L. T.; Itzkan, I.; Dasari, R. R.; Feld, M. S. *Phys. Rev. Lett.* **1997**, *78*, 1667–1670.
(18) Nie, S.; Emory, S. R. *Science* **1997**, *275*, 1102–1106.
(19) Xu, H.; Bjerneld, E. J.; Käll, M.; Börjesson, L. *Phys. Rev. Lett.* **1999**, *83*, 4357–4360.
(20) Futamata, M.; Maruyama, Y.; Ishikawa, M. *Vib. Spectrosc.* **2002**, *30*, 17–23.
(21) Lyon, L. A.; Keating, C. D.; Fox, A. P.; Baker, B. E.; He, L.; Nicewarner, S. R.; Mulvaney, S. P.; Natan, M. J. *Anal. Chem.* **1998**, *70*, 341–362.
(22) Vo-Dinh, T. *Trends Anal. Chem.* **1998**, *17*, 557–570.
(23) Rohr, T. E.; Cotton, T.; Fan, N.; Tarcha, P. J. *Anal. Biochem.* **1989**, *182*, 388–389.
(24) Marc, D. P.; Robert, J. L.; Lorraine, M. S.; Gufeng, W.; Radha, N. *Chem. Soc. Rev.* **2008**, *37*, 1001–1011.
(25) McCabe, A. F.; Eliasson, C.; Prasath, R. A.; Hernandez-Santana, A.; Stevenson, L.; Apple, I.; Cormack, P. A. G.; Graham, D.; Smith, W. E.; Corish, P.; Lipscomb, S. J.; Holland, E. R.; Prince, P. D. *Faraday Discuss.* **2006**, *132*, 303–308.
(26) Yu, K. N.; Lee, S. M.; Han, J. Y.; Park, H.; Woo, M. A.; Noh, M. S.; Hwang, S. K.; Kwon, J. T.; Jin, H.; Kim, Y. K.; Hergenrother, P. J.; Jeong, D. H.; Lee, Y. S.; Cho, M. H. *Bioconjugate Chem.* **2007**, *18*, 1155–1162.
(27) Jun, B. H.; Kim, J. H.; Park, H.; Kim, J. S.; Yu, K. N.; Lee, S. M.; Choi, H.; Kwak, S. Y.; Kim, Y. K.; Jeong, D. H.; Cho, M. H.; Lee, Y. S. *J. Comb. Chem.* **2007**, *9*, 237–244.
(28) Campion, A.; Gallo, A. R.; Harris, C. B.; Robota, H. J.; Whitmore, P. M. *Chem. Phys. Lett.* **1980**, *73*, 447–450.
(29) Kümmerlen, J.; Leitner, A.; Brunner, H.; Aussenegg, F. R.; Wokaun, A. *Mol. Phys.* **1993**, *80*, 1031–1046.
(30) Sokolov, K.; Chumanov, G.; Cotton, T. M. *Anal. Chem.* **1998**, *70*, 3898–3905.
(31) Lakowicz, J. R. *Anal. Biochem.* **2001**, *298*, 1–24.
(32) Lakowicz, J. R.; Shen, Y.; D'Auria, S.; Malicka, J.; Fang, J.; Gryczynski, Z.; Gryczynski, I. *Anal. Biochem.* **2002**, *301*, 261–277.
(33) Desaja-Gonzalez, J.; Aroca, R.; Nagao, Y.; DeSaja, J. A. *Spectrochim. Acta, Part A* **1997**, *53*, 173–181.
(34) Geddes, C. D.; Lakowicz, J. R. *J. Fluoresc.* **2002**, *12*, 121–129.
(35) Aroca, R. F.; Constantino, C. J. L. *Langmuir* **2000**, *16*, 5425–5429.
(36) Dos Santos, D. S., Jr.; Aroca, R. F. *Analyst* **2007**, *132*, 450–454.
(37) Smith, D. S.; Kostov, Y.; Rao, G. *Sens. Actuators, B: Chem.* **2007**, *127*, 432–440.
(38) Sabanayagam, C. R.; Lakowicz, J. R. *Nucleic Acids Res.* **2007**, *35*, e13.
(39) Kim, K.; Lee, H. B.; Lee, Y. M.; Shin, K. S. *Biosens. Bioelectron.* **2009**, *24*, 1864–1869.
(40) Stöber, W.; Fink, A.; Bohn, E. *J. Colloid Interface Sci.* **1968**, *26*, 62–69.
(41) Richter, B.; Kirstein, S. *J. Chem. Phys.* **1999**, *111*, 5191–5200.
(42) Singamaneni, S.; Jiang, C.; Merrick, E.; Kommireddy, D.; Tsukruk, V. V. *J. Macromol. Sci., Part B: Phys.* **2007**, *46*, 7–19.
(43) Sato, H.; Kidaka, T.; Hori, M. *Appl. Biochem. Biotechnol.* **1987**, *15*, 145–158.
(44) Tuong, S. D.; Kim, H.; Lee, H. *Macromol. Res.* **2008**, *16*, 373–378.
(45) Wang, C.; Chen, Y.; Wang, T.; Ma, Z.; Su, Z. *Adv. Funct. Mater.* **2008**, *18*, 355–361.
(46) Halthur, T. J.; Claesson, P. M.; Elofsson, U. M. *J. Am. Chem. Soc.* **2004**, *126*, 17009–17015.
(47) Kim, K.; Kim, H. S.; Park, H. K. *Langmuir* **2006**, *22*, 8083–8088.
(48) Kim, K.; Lee, H. S.; Yu, H. D.; Park, H. K.; Kim, N. H. *Colloids Surf. A* **2008**, *316*, 1–7.
(49) Huang, P.-J.; Chau, L.-K.; Yang, T.-S.; Tay, L.-L.; Lin, T.-T. *Adv. Funct. Mater.* **2009**, *19*, 242–248.
(50) Sanles-Sobrido, M.; Exner, W.; Rodríguez-Lorenzo, L.; Rodríguez-González, B.; Correa-Duarte, M. A.; Álvarez-Puebla, R. A.; Liz-Marzán, L. M. *J. Am. Chem. Soc.* **2009**, *131*, 2699–2705.
(51) Bruchez, M., Jr.; Moronne, M.; Gin, P.; Weiss, S.; Alivisatos, A. P. *Science* **1998**, *281*, 2013–2016.
(52) Nam, J.-M.; Park, S.-J.; Mirkin, C. A. *J. Am. Chem. Soc.* **2002**, *124*, 3820–3821.
(53) Battersby, B. J.; Bryant, D.; Meutermans, W.; Matthews, D.; Smythe, M. L.; Trau, M. *J. Am. Chem. Soc.* **2000**, *122*, 2138–2139.
(54) Cunin, F.; Schmedake, T. A.; Link, J. R.; Li, Y. Y.; Koh, J.; Bhatia, S. N.; Sailor, M. J. *Nat. Mater.* **2002**, *1*, 39–41.
(55) Han, M.; Gao, X.; Su, J. Z.; Nie, S. *Nat. Biotechnol.* **2001**, *19*, 631–635.
(56) Vaino, A. R.; Janda, K. D. *Proc. Natl. Acad. Sci. U.S.A.* **2000**, *97*, 7692–7696.
(57) Dickinson, T. A.; Michael, K. L.; Kauer, J. S.; Walt, D. R. *Anal. Chem.* **1999**, *71*, 2192–2198.

AM9003396